Combustion and Flame 205 (2019) 180–192

Contents lists available at ScienceDirect

Combustion and Flame

journal homepage: www.elsevier.com/locate/combustflame

Soot inception in laminar coflow diffusion flames

Daniel Bartos[a,*], Mariano Sirignano[b], Matthew J. Dunn[a], Andrea D'Anna[b], Assaad Rachid Masri[a]

[a] School of Aerospace, Mechanical and Mechatronic Engineering, The University of Sydney, NSW 2006, Australia
[b] Dipartimento di Ingegneria Chimica, dei Materiali e della Produzione Industriale, Universita'degli Studi di Napoli Federico II, Napoli, Italy

ARTICLE INFO

Article history:
Received 14 March 2018
Revised 12 June 2018
Accepted 20 March 2019
Available online 15 April 2019

Keywords:
Nanostructures
Nanoparticles
Soot
Laser-induced fluorescence
Laser-induced incandescence
Laminar diffusion flame

ABSTRACT

This paper focuses on the soot inception region in laminar coflow diffusion flames of methane and ethylene stabilised on the Yale diffusion burner. Earlier studies of these flames have focused on the downstream regions where soot has already developed. Laser-induced fluorescence (LIF) and elastic scattering measurements from 266 nm excitation are combined with laser-induced incandescence (LII) excited at 1064 nm. The structure and evolution of the soot precursor particles are characterised using the LIF intensity, decay time and the relative spectral emission in the ultraviolet and visible. The LIF decay times indicate that the majority of 266 nm excited LIF originates from nanostructures rather than gas phase polycyclic aromatic hydrocarbons (PAH). A similarity in the particle evolution for the low and high sooting flames in the upstream regions is found, indicating a general transition towards larger structures with more aromatic features as the nanostructures advect downstream in the fuel rich pyrolytic conditions. Higher nanostructure concentrations are found to precede the higher soot volume fractions (SVF) found in fuel rich sootier flames, although not proportionally, suggesting that surface growth strongly contributes to SVF in the high sooting flames. In the heavier sooting flames the majority of particle formation shifts from the centreline to the wings at the outer edges of the flame closer to stoichiometry. Particle formation in the wings of the flames occurs in the presence of oxygen and higher temperatures, resulting in particles with spectroscopic properties resembling those formed toward the oxidiser side of counter-flow diffusion flames. In the heavier sooting flames, particles produced in the wings appear to mix with particles formed along the centreline of the flame at the flame tip, resulting in a broad range of nanostructures and soot occurring in this region.

1. Introduction

Understanding the mechanism of particle formation in flames, particularly in the inception stages, remains an outstanding challenge despite extensive research that has already been published on this topic [1–4]. The difficulty is multi-layered and lies in the moieties of the species present in the gas phase, many of which are polycyclic aromatic hydrocarbons (PAH), the transition from molecular to solid nanostructures and hence to soot, and the difficulty of probing these domains. In recent years, studies have focused on characterising particles based on their physico-chemical features [1,5–13]. In this context, it is important to have clear terminology that define the nomenclature of combustion-generated carbonaceous particles. In this paper, the term "soot" is used to refer to both primary particles and aggregates defined by their ability to absorb infrared light and incandesce [14–18]. Conversely, the term "nanostructures" is attributed to other species in a condensed state (i.e. both solid and/or liquid-like but not in gas phase) possessing no broadband absorption features in the infrared and the ability to fluoresce under ultraviolet (UV) excitation [5–7,19]. It is important to underline that, although the fluorescence from these nanostructures is from aromatic groups, a key distinction is made between gas phase PAH and those bound in nanostructures. Finally, it is believed that mechanisms that dominate combustion-generated particle evolution may differ between premixed and non-premixed modes hence the necessity to study both modes of combustion [1], where this paper focuses on the non-premixed mode.

In laminar premixed flames, combustion-generated particles have been studied extensively using a range of diagnostic methods particularly laser-induced fluorescence (LIF) and laser-induced

Abbreviations: ELS, Elastic light scattering; HAB, Height above burner; ISF, International sooting flame (Workshop); LIE, Laser-induced emission; LIF, Laser-induced fluorescence (LIE attributable to fluorescence); LII, Laser-induced incandescence (LIE attributable to incandescence); NOC, Nano-organic carbon; PAH, Polycyclic aromatic hydrocarbon; PMT, Photomultiplier tube; SVF, Soot volume fraction; TRFPA, Time-resolved fluorescence polarization anisotropy; UV, Ultraviolet; UV/VIS, UV to visible LIF ratio (PMT2/PMT3); LL, Lower limit of LIF signals corrected for SVF interference.

* Corresponding author.
E-mail address: dbar4475@uni.sydney.edu.au (D. Bartos).

https://doi.org/10.1016/j.combustflame.2019.03.026
0010-2180/

incandescence (LII). LII is generally attributed to soot particles and aggregates in the order of tens to hundreds of nanometres that are sufficiently graphitic to be heated up to temperatures of 3500–4500 K [4,14–18]. The minimum particle size threshold below which LII can no longer be detected remains an open question and subject to current research [4,20,21]. LIF, on the other hand, can be observed from molecular PAH and has also been detected from soot precursors, in the range of sizes between the largest gas phase PAHs and the smallest solid particles tracked by LII. It is noted here that soot precursor particles are also often referred to as condensed phase, nanostructures, nanoparticles or nano-organic carbon (NOC) that exhibit physical and chemical properties somewhere between those of large aromatic molecules and solid particles [22]. Time-resolved 266 nm excited LIF measurements have been shown to be able to delineate between LIF from PAH and LIF originating from nanostructures, LIF-PAH decay times decrease rapidly at flame temperatures to hundreds of picoseconds [23], whereas LIF decay time from nanostructures at flame temperatures remain long, typically greater than 2 ns [24,25].

A recent application of time-resolved LII-LIF to laminar premixed flames with a range of C/O ratios has shown that the temporal decay times of the LIF signals are much longer than those expected for molecules at the same temperature, yet much shorter and spectrally different than those of soot particles [24]. It was concluded that LIF is able to track nanostructures as condensed phase matter with sizes in the order of few nanometres and with internal structures exhibiting the spectroscopic behaviour of small PAHs. The condensed state of these nanostructures enhances their quantum yield resulting in a longer decay time consistent with experimental findings. On the other hand, the low quantum yield of gas phase PAH reduces their contribution to the LIF signal, to negligible levels in certain conditions [19]. Such nanostructures described and detected by LIF are found to be compatible with other experimental findings, employing multiple techniques [5–13].

In diffusion flames, the dominant transport processes and the structure of the reaction zones are different from those in the premixed flames and this may impact the mechanism of particle inception [1–4,25]. Combustion-generated particle formation in laminar non-premixed flames has been studied in burner configurations ranging from planar [26] to circular [27–30] to counterflow [25,31–33]. More recently, the axisymmetric burner developed at Yale University, heron referred to as the “Yale burner”, has become an accepted target flame platform adopted by the International Sooting Flame Workshop (ISF) [34]. Existing measurements in sooting flames stabilised on the Yale burner have focused on the downstream structure of soot rather than the particle inception process [35]. The purpose of this paper is, therefore, to fill this gap and shed light on the mechanism of particle inception in the Yale diffusion flames through the application of time-resolved LIF-LII. The use of different fuels, namely methane and ethylene, allows the investigation to span a large range of sooting conditions, testing the adopted technique, and at the same time exploring the inception process in a broad selection of operative conditions. The high aspect ratio flames (defined as the ratio of the visible flame length over the jet diameter) produced by the Yale burner also provide an opportunity to investigate conditions where separation of the centreline and the edge of the flame is relatively small, hence diffusion between these two regions may be significant. Discussion and comparisons are made, where relevant, with previous measurements and calculations of the flames examined.

2. Experimental setup

The burner configuration adopted here was the Yale burner and it consists of a 4 mm ID jet for the fuel mixture (methane or ethylene mixed with nitrogen) surrounded by a 74 mm diameter coflow of air. A detailed description of the burner may be found elsewhere [34,36,37]. A number of different sooting propensities were examined from marginally sooting methane flames [38] to obviously sooting ethylene flames [35,39], with details of the investigated flames presented in Table 1 and photos presented in Fig. 1. All but the M80 flame were target flames for the ISF [34]. The choice of flow rates for M80 was made in order to compare the results obtained with ethylene in similar conditions of carbon flow rate. For the naming convention, the “M” and “E” represent methane and ethylene respectively, while the following number corresponds to the percent fuel in the jet mixture. The cold bulk velocity for all flames was 35 cm/s for both the jet mixture and the coflow. Time-resolved, pointwise laser-induced emission (LIE) measurements were conducted along the centreline of the flames, and some select radial traverses were also conducted for the ethylene cases.

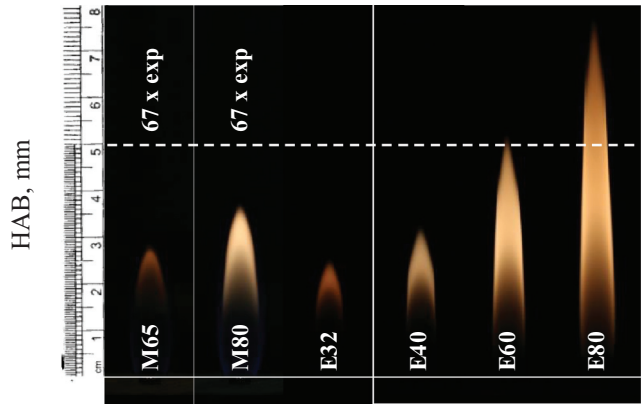

Fig. 1. Photographs of all flames. All photographs were taken at same $f_{\#}$ and exposure except for those labelled with extended exposure. (For interpretation of the references to colour in this figure, the reader is referred to the web version of this article.)

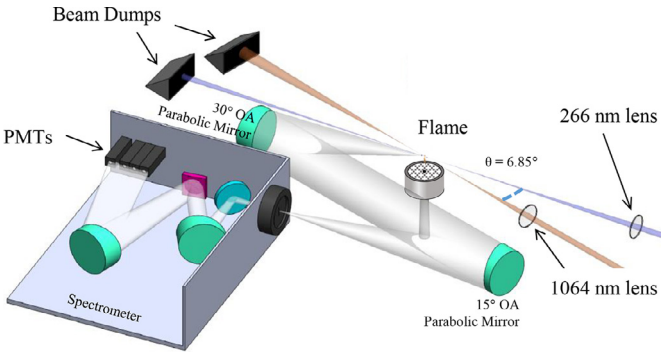

Fig. 2. Experimental setup and optical layout.

2.1. Time-resolved LIF-LII

The experimental setup used has been described in detail in previous works [24,40], and therefore only essential details are given here. The flames were probed with two different laser sources, namely a 266 nm, 80 ps duration UV pulse and a 1064 nm, 8 ns duration IR pulse as shown in Fig. 2. The UV was the first pulse and was generated by the 4th harmonic (266 nm) of a mode-locked Nd:YAG 10 Hz pulsed laser (Ekspla PL2251 Series Laser). The UV beam focus was measured to have a 250 μm diameter resulting in a fluence level of 1.2 J/cm^2. The use of picosecond pulses (compared to earlier measurements using a typical 8 ns pulse [25]) is necessary to avoid distortion of the short LIF decay times expected from fluorescing species at high temperatures [23]. The fluence for

Table 1
Details of flames investigated.

Flame	Fuel	Fuel (CH_4 or C_2H_4) flow rate, SLPM	Fuel dilution (N_2) flowrate, SLPM	Air coflow flowrate, SLPM	Carbon flowrate g_C/min	Flame length (mm)
M65	CH_4	0.172	0.092	90	0.084	28
M80	CH_4	0.211	0.053	90	0.103	37
E32	C_2H_4	0.084	0.179	90	0.082	25
E40	C_2H_4	0.106	0.158	90	0.103	32
E60	C_2H_4	0.158	0.106	90	0.154	50
E80	C_2H_4	0.211	0.053	90	0.206	74

the UV laser pulse was chosen to maximise the LIF signal with respect to the interference (see later in the text) originating from undesired phenomena such as photofragmentation or soot ablation. The fluence is similar to that reported in previous work where the time decay of LIF from nanostructures was compared to that of PAH (0.8 J/cm^2) [25], and is also comparable with other time-resolved fluorescence polarisation anisotropy (TRFPA) experiments conducted in the past based on the energy pulse and the presumed spot size [41–43]. The second laser, the IR, was generated by the fundamental output (1064 nm) of a 10 Hz, Nd:YAG pulsed laser (Spectra-Physics Quanta-Ray Pro-350) and was used to excite LII from soot exclusively. The IR probe diameter was measured to be 450 µm resulting in a fluence level of 0.6 J/cm^2. The choice of both UV and IR fluence was made on the basis of accepted values in literature on this topic and values previously used in laminar premixed flames as well as turbulent piloted jet flames [24,40]. In this study, the UV pulse preceded the IR pulse by 900 ns, which is different and significantly longer than previous work [24,40]. The UV to IR temporal separation time of 900 ns is still short relative to the advection times in the flow, and thus the same gas volume was irradiated by both the UV and IR pulses permitting the possibility of newly formed particles from laser ablation and sublimation of soot [44–46] affecting the particle morphology and particle size distributions [47]. Previous measurements in premixed flames [24] have examined the potential interference between the UV and IR beams in detail for shorter inter-pulse durations in premixed flames and found no discernible interaction. Although not explored in detail in this paper, the authors found no difference in the LII signal with or without the UV beam present in the axial traverse for the E60 flame for the inter-pulse duration utilised in this work. The LII measurements reported in this paper also show strong agreement with previously published soot volume fraction (SVF) measurements [35,39], indicating that if any interaction had occurred such as sublimation from the smallest soot particles, it had no noticeable impact on the SVF measurement [44].

The collection system consisted of four fast photomultiplier tubes (PMTs) (Hamamatsu H10721-210 and H10721-20) situated at the focal plane of a 1/2 m spectrometer. The four PMTs simultaneously collected time-resolved signals in four distinct spectral bands: PMT1 @ 266 ± 15 nm, PMT2 @ 350 ± 15 nm, PMT3 @ 445 ± 15 nm, PMT4 @ 575 ± 15 nm. PMT1 was used to capture elastic light scattering (ELS) from the laser pulse at 266 nm. PMT2 and PMT3 were used to measure LIF in the UV and the visible spectral range; the choice of these two spectral bands was made in accordance to the observed broadband LIF seen in previous works [25,29,31,48–52]. Finally, PMT4 was dedicated primarily to monitor LII, although some LIF could be present depending on the local soot and nanoparticle concentrations. The LII on PMT4 could be from either the 266 nm or 1064 nm laser pulses, producing a quasi-blackbody emission curve extending down to wavelengths in the UV, (PMT2 and PMT3). The placement of the PMTs at these spectral bands also avoided the majority of known carbon cluster interferences [53]. However, in regions of the flame where a high soot volume fraction (SVF) was detected, some interferences from carbon clusters may be present. An important distinction to be made here is that LIE refers to the total Laser-Induced Emission, known or unknown, collected by the PMTs. LIF, on the other hand, is used in reference to all or part of that signal which can be attributed to Laser-Induced Fluorescence. A constant gain for all the PMTs was used in this study, with the gain level set to maximise the signal level yet prevent any signal saturation in all the flames examined. Using a constant gain level minimises differences in the systems impulse response which varies with gain, and minimises any day-to-day systematic errors, allowing easy comparison of results between flames. However, the mentioned advantages of a constant PMT gain are at the expense of a reduced dynamic range, hence a decreased sensitivity to what is theoretically possible from the system when measuring in flames with either low soot, low fluorescence or low scattering levels. The signals from the four PMTs were recorded using a high sample-rate (25 Giga-samples/s), high bandwidth (4 GHz) oscilloscope (Tektronix DSA70404C).

Light from the probe volume was focused onto the vertically oriented 20 µm spectrometer slit by a series of two 4-inch parabolic mirrors collecting at 30 degrees off parallel to the laser path. A 280 nm high-pass filter was placed in front of the spectrometer slit to attenuate approximately 98% of the 266 nm scattering. ELS was by far the most intense emission observed in this study and changed by several orders of magnitude between gas phase scattering and large soot scattering. All results presented in this paper were corrected to account for the spectral response of the system, including the UV filter, allowing direct comparisons to be made between the different wavelength PMT signals. The spectral calibration of the system was performed using a broadband emitting deuterium lamp light source dispersed through a monochromator, the output of which was calibrated by a NIST traceable photodiode. At each measurement location, 500 acquisitions were recorded and subsequently averaged. The resultant collection system was very sensitive, able to detect SVFs in the order of 10 ppb, but was also able to measure ELS, LIF and LII signals ranging over orders of magnitude from non-sooting to heavily sooting conditions. SVF presented in the present work was calculated through a linear correlation of the 1064 nm LII measurements and previous measurements in the same ethylene flames, whose data sets are available on the ISF website [34] from the Yale group [35]. While this method does not take into account the impact of temperature, the supplementary material provides a discussion on the limited impact this has.

3. Results and discussion

3.1. Signal processing

A typical 500 shot average temporally-resolved signal measured with PMT3, i.e., in the visible region of the LIF, in a zone where no 1064 nm LII was detected is shown in Fig. 3. For the flames studied, multiple signals, including LIF and LII, often coexist and hence contribute to the peak value of the signal in varying proportions. The interference between different signals also impacts the temporal location of the peak signal due to the different time evolutions of these processes in different locations and flames. In fact,

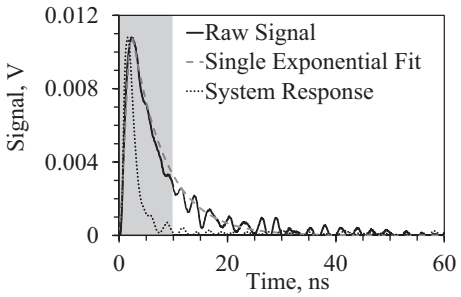

Fig. 3. LIF Signal against time measured by PMT3 @ 445 nm in M65 at HAB = 22 mm (Solid) alongside single exponential decay fit (dashed) and measured system response (dotted). Also presented is the area considered for "prompt" signal (shaded).

in Fig. 3 the location of the peak is slightly delayed in the LIF signal (solid line) with respect to the pure scattering - i.e. the system response denoted by the dotted line, due to the longer decay time of the fluorescence process.

In order to track and compare the UV excited LIE signal across all the flame conditions, a metric related to the temporally integrated signal is required. All UV excited signals reported in this paper are based on a "prompt" signal which is defined as the integral from 0 to 10 ns. This "prompt" approach allows the analysis of the component of the UV excited signal that is weighted towards fluorescence which possess relatively short decay times, rather than the longer LII decay times. The prompt signal is not sensitive to the small variations in the rise and fall times for the LIF and LII components of the signal. Hence the prompt signal employed here provides a more consistent approach to comparing the UV excited fluorescence at different locations and different flames, compared to simply utilising the peak or the integral of the total signal. The prompt portion of the signal shown in Fig. 3 is mainly composed of short-lived signals that exhibit a fast exponential-like decay. The prompt signal is reported in this paper is in units of V.ns (volts × nanoseconds), where the voltage produced by each PMT is corrected for the spectral throughput. The small amplitude ringing artefacts shown in Fig. 3, evident at times >10 ns, are due to transmission line effects generated by the impulsive nature of the signal. The node locations of the ringing artefacts in time are repeatable; hence they are present in the average signal shown in Fig. 3. The ringing artefacts do not impact any of the results or conclusions presented in this paper and are always a small component of the signal.

The decay time of the signal is an important metric as it permits the attribution of the signal to broad classes of molecules or particles. A mono-exponential (convoluted with the system response) fitting approach has been applied to the data presented in this paper to determine the characteristic signal decay time. Whilst a bi-exponential fit has been used in previous work, a single exponential is more than sufficient for the flame conditions and locations presented in this paper where LII free LIF signals present no obvious bi-exponential features. A maximum error of 18% was found comparing a mono-exponential fit with the bi-exponential fit used previously in flat premixed flames [24]. Regions of the flames where the UV and visible LIE signals are strongly bi-exponential, such as in the high sooting region, specific decay times are not presented in these regions due to challenges of separating the components belonging to LIF, LII and possibly other phenomena.

3.2. Methane flames

LIE measurements along the centrelines of both the M65 and M80 methane flames are presented versus height above burner (HAB) in Fig. 4(a) and (b), respectively, with the corresponding LIF decay times reported in Fig. 4(c) and (d). The centreline profile of temperature is reported for flame M65 in Fig. 4(c) based on the computations by Walsh et al. [54]. These computations of temperature and major species were found to agree well with Rayleigh thermometry measurements reported by Kempema et al. [38]. The M65 flame has a small, orange, low-luminosity tip from 23 to 28 mm HAB, indicating the presence of soot, albeit at low concentrations (see Fig. 1). LII resulting from 1064 nm excitation is shown in Fig. 4(a) for the M65 flame, with the results suggesting that the local soot concentration is below the detection limit. The very low soot concentration in the M65 flame shows that it is a good flame to analyse the trend of the fluorescence intensity and decay time vs. HAB due to the very low potential interference effects from soot. The generation of the LIF signal above the background for the M65 flame begins at HAB = 10 mm, then increases at the same HAB where a rise in temperature is found in Fig. 4(c), indicating that the LIF signal is correlated with heat-releasing reactions in the flame. The LIF intensity, both at 350 nm and 445 nm in Fig. 4(a) continues to increase with HAB towards the end of the flame before dropping off in the oxidation zone.

UV excited LIF in sooting or near sooting flames, such as the M65 flame in Fig. 4(a) has often been attributed to PAH molecules known to form in the soot inception region [3,29,30,55]. Utilising previous measurements of PAH fluorescence decay time as a function of temperature, the measured fluorescence decay time and the flame temperature, it is possible to assess if the UV excited LIF in the high aspect ratio diffusion flames explored in this paper are due to PAH. Utilising the temperature and the PAH decay time measurements of Ossler et al. [23], the decay times of naphthalene, fluorene, anthracene and pyrene are plotted at the corresponding temperatures within the flame as shown in Fig. 4(c). A broad region representing the range of fluorescence decay times expected from PAH considering the variation of the decay time for different species and the temperature is shown in Fig. 4(c) shaded in grey. Decay times for PAH larger than pyrene are not considered as their quantum efficiency, spectral emission and fluorescence decay time are not expected to be significantly different, and most probably exist in smaller concentrations, compared to the four representative PAH considered here [56,57]. The presence of strong quenching species such as O_2 and H_2O will only decrease the predicted PAH fluorescence decay times shown in Fig. 4(c), although along the centreline the presence of O_2 is considered negligible. From the predicted PAH decay times shown in Fig. 4(c), a rapid decrease fluorescence decay time with temperature is predicted, with decay times less than 1 ns at temperatures approaching 1200 K.

Measured decay times for the M65 flame are shown in Fig. 4(c) vs. HAB for both LIF at 350 nm and 445 nm, with decay times ranging from 2 ns near the burner exit to 8 ns near the end of the flame. In the low-temperature region of the flame at HAB < 10 mm, the measured decay times of 2–4 ns are much smaller than the expected PAH decay times of 10–100 ns. In the absence of strong quenchers such as oxygen, an explanation for the short decay time at HAB < 10 mm could be due to CH_4 being a strong PAH quencher or the bulk of the UV LIF excited signal to not be due to PAH. Multiphoton photofragmentation of methane from 266 nm excitation is expected to be a very small contributor to the signal in the methane flames. However, due to the very low LIE signal levels in the M65 flame, it can be seen in Fig. 4(a) that for HAB ≤ 8 mm, some of the 445 nm LIE signal could possibly be attributed to CH_4 photofragmentation. The lower temperature and thus presence of unburned CH_4 in this region likely contributes to this emission. From HAB 10–18 mm where the temperatures are less than 1000 K, the measured fluorescence decay times correspond to similar decay times expected from PAH. For HAB > 18 mm the measured decay times range from 5 to 8 ns and these are much longer

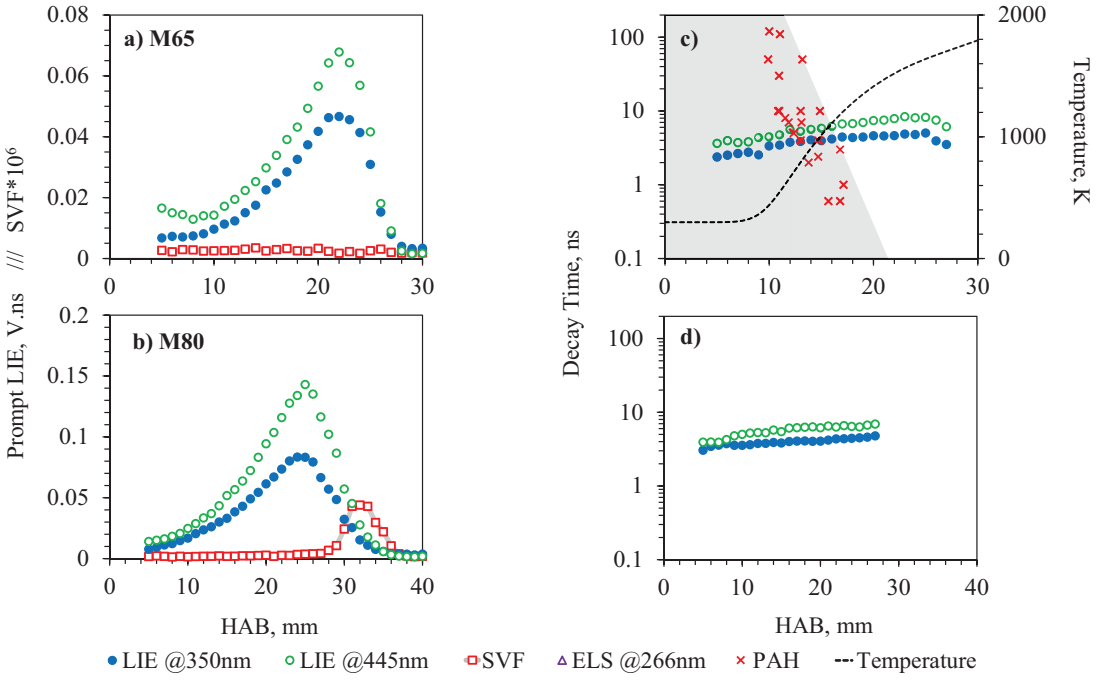

Fig. 4. (a) and (b) Prompt LIE and SVF centreline measurements against HAB in methane flames. (c) and (d) Measured LIF decay times plotted alongside molecular PAH decay times (τ_{eff}) measured by Ossler et al. [23] corresponding to the computed temperature of the flame from the work of Walsh et al. [54].

than the sub 1 ns decay times predicted for PAH at these temperatures. The significant difference in decay time indicates that the origin of the fluorescence certainly in the high-temperature region of the flame is from similar nanostructures found previously in premixed flames [24]. Hence the increase in LIF cannot be solely explained by a concentration increase of PAH because of the corresponding increase in decay time seen in Fig. 4(c). Previous measurements using time-resolved fluorescence polarisation anisotropy (TRFPA) [41–43] have also confirmed the presence of fluorescent particles with much larger effective diameters than molecular PAH in non-sooting regions of diffusion and premixed flames.

Both the 350 nm and 445 nm emission show similar trends for both the LIF prompt emission and the fluorescence decay time for all HAB despite the large temperature changes. It seems reasonable to hypothesise that the nanostructures concluded to be responsible for the LIF for HAB > 18 mm are the same source of the fluorescence emission for HAB < 18 mm, thus ruling out PAH emission as the source. Fluorescence decay times are function of several variables including temperature, the concentration of quenching species and particle structure [23,25,58] and thus attempts to attribute decay times to an average particle size would be speculative, without further information. However, it would be reasonable to assume that these nanostructures are somewhere between 1 nm and 10 nm diameter as previously observed in both lower aspect ratio diffusion [42,43] and premixed flames [24,41].

The centreline LIF measurements for the M80 flame, shown in Fig. 4(b), feature very similar centreline trends to the M65 flame, with the exception of a detectable SVF. The M80 flame is visibly sooting, with 1064 nm excited LII observed from HAB = 29 mm to the tip at 37 mm. In the sooting region of the M80 flame, the LIE signals from 266 nm become a combination of LIF, LII and potential interferences from sublimated species such as C_2 and C_3 [53]. The impact of the emerging 266 nm LII signal results in a steep increase in decay time measured where LII is detectable. Interpreting the decay time in the sooting region becomes difficult and the current method is no longer appropriate due to obvious multi-exponential components to the signal. For this reason, decay times are not presented in these regions (HAB > 28 mm) where multiple LIEs contribute to the signal. Metrics that rely on longer integration times, such as the decay times are greatly affected by the LII component of the signal. However, the prompt part of the signal as used in Fig. 4(b) is still very much dominated by LIF in this low sooting flame. Prior to the onset of soot, the decay time for the M80 flame in Fig. 4(d), displays a trend of increasing LIF decay time with increasing temperature, similar to the M65 flame. Even though temperature measurements are not available for this flame, the temperature profile can be expected to be similar to that seen in M65. In the high-temperature regions of the flame the LIF decay times in this flame are again much larger than that expected of molecular PAH at high temperatures, and thus can be attributed to nanostructures.

Based on the rise and fall of LIF intensity in M65 and M80 flames, some similarities and some differences can be observed. The LIF signal increase is quite similar in terms of slope once normalised by the maximum value, which suggests that, as expected, the formation process in both flames involves similar pathways. However, it is interesting to note that in the M65 flame where no LII is detected the LIF signal rapidly decreases approaching the oxidation zone and thus the end of the flame. On the other hand, in the M80 flame, the LIF appears to decrease at a lower rate with respect to HAB, suggesting that the small nanostructures are converted to soot before the oxidation zone and only afterwards the global oxidation takes place. No ELS was detected above the system sensitivity limit for both M65 and M80 flames despite there being a detectable, albeit small, amount of soot from 1064 nm excited LII found in the M80 flame. Further measurements with higher sensitivity would be required to determine if any emissions in the region of 250–280 nm, i.e. in the spectral detection range of PMT1, are due to elastic scattering or LIF, which is known to extend down to at least 280 nm [25].

3.3. Ethylene flames

Using a similar methodology as in Section 3.2, LIE measurements along the centreline of ethylene flames are presented in Fig. 5. Due to the wavelength and intensity of the 266 nm

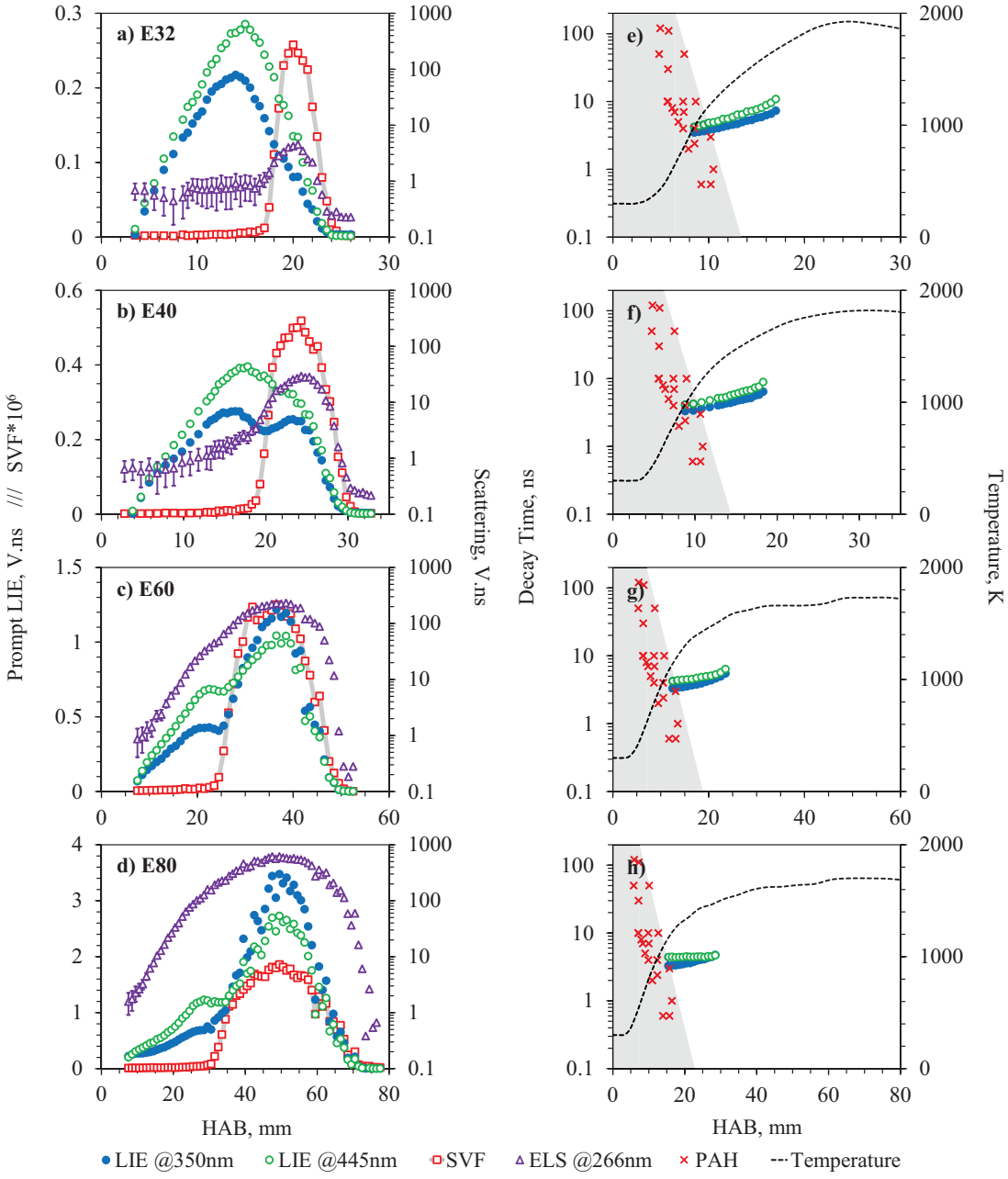

Fig. 5. (a)–(d) Prompt LIE and SVF centreline measurements against HAB in ethylene flames. (e)–(h) Measured LIF decay times plotted alongside molecular PAH decay times (τ_{eff}) measured by Ossler et al. [23] corresponding to the computed temperature of the flame from the work of Smooke et al. [35].

laser used, photofragmentation of ethylene was observed close to the burner exit producing a signal proportional to ethylene concentration on all the PMTs. It is worth noting that the photofragmentation and subsequent fluorescence yield interference for ethylene is larger than methane and thus the interference in the first part of the ethylene flames is much stronger than the methane flames. Assuming that 100% of the LIE signal recorded by all PMTs before the reaction zone is due to photofragmentation, the prompt signals are corrected based on ethylene concentration and consumption calculated using the computed temperature taken from the work of Smooke et al. [35]. The prompt signal correction method employed does not remove any contribution of the ethylene fragmentation signal on the temporal decay. To avoid erroneous interpretation in Fig. 5, decay times have been excluded for the ethylene flames close to the jet exit plane where signals are expected to be impacted by the presence of photofragmentation. Additionally, due to the higher sooting propensity of ethylene flames, the prompt LIF and LIF decay times in the downstream regions are also challenging to interpret due to the presence of interferences from soot. As with the M80 flame, the decay times deemed to be impacted by LII are omitted. In all of the ethylene flames investigated LII has been detected, which is not surprising due to the higher sooting propensity of ethylene compared to methane. Unlike the methane flames, ELS is detected above the system sensitivity for all of the ethylene flames and shown in Fig. 5 on a logarithmic scale to enable trends in ELS to be observed over a wide dynamic range. Error bars are placed on the ELS measurements presented in Fig. 5 to show the potential LIF contribution to the ELS signals. It is known that LIF signals extend down deep into the UV [25], around 280 nm, and thus can be present on PMT1. In sooting regions of all flames, this deep UV fluorescence signal contributes negligibly to the ELS signal. However, at

low HAB where ELS is low, and LIF signals are at their peak, the interference of LIF on PMT1 can be significant.

For the lowest ethylene concentration case, the E32 flame reported in Fig. 5(a) and (e), some similarities in the LIF profile compared to M80 can be seen: LIF reaches a maximum (around HAB = 14 mm for the E32 flame) before the occurrence of soot and continues to decrease with HAB when soot is detected with LII (at HAB = 18 mm for the E32 flame). The LIF signal decays to the background level at the end of the oxidation region at the same HAB where no more LII from soot is present in both flames. Despite the broad similarities of the structure of the LIF vs. HAB for the E32 and M80 flames, the E32 flame features LIF intensities double those of the M80 flame and SVF levels approaching an order of magnitude greater than the M80 flame. The increased soot formation results for the E32 flame indicate that while coagulation of smaller nanoparticles is important for continued soot growth, the mechanisms of surface growth are becoming more dominant in the ethylene flames. A detectable ELS signal is evident in the E32 flame, with uniform scattering signal in the non-sooting region where no LII is detected, progressing to a peak that correlates with the location and width of the sooting region.

Measurements in the E32 flame highlight the signal valley created between the peaks of UV LIF and LII signals, often referred to as the “dark region”, which has been observed in a number of studies [29,30,59,60]. The rapid decrease of UV LIF before the occurrence of soot shows a strong resemblance to the trend of UV absorbing nano-organic carbon (NOC) measurements conducted by D’Anna et al. [27] in diffusion flames that have a particle size range estimated to be between 2 nm and 4 nm. Complementary investigations by the Naples group [42,43] show that particles in this “dark region” have a higher quantum yield at longer wavelengths, compared to the nanostructures observed upstream of this region. Consequently “dark region” particles exhibit longer fluorescence emission wavelengths and have sizes up to 20 nm measured through TRFPA [42]. Relative to the marginally sooting methane flames, the ethylene flames feature higher fluorescence intensities and longer fluorescence decay times. Considering that the fluorescence signal from nanoparticles can be considered to be proportional to the volume concentration of nanoparticles [61] or alternatively to the number concentration if a fixed mean particle size is assumed, the significantly higher LIF signals found in the ethylene flames compared to the methane flames may be attributed to a greater nanoparticle concentration. By virtue of the higher nanoparticle concentrations in the ethylene flames, particle coagulation rates will be increased, creating larger particles that are still capable of fluorescence emission. The enhanced production of larger nanoparticles in the ethylene flame compared to the methane flames agrees with the findings of longer decay times in the ethylene flames.

Moving from the E32 flame to the higher sooting E40, E60, and E80 flames, a strong increase in the ELS signal is noted with HAB in the regions where no soot is detected, as shown in Fig. 5(b)–(d). The rapid initial increase in ELS with HAB in the non-sooting region of the flame along the centreline is faster than the growth of the LIF signal and suggests that in the early zone of a diffusion flame, it is possible to find fluorescing nanostructures with sizes that can vary from about 2 to 20 nm [42] which would contribute to a significant ELS signal in excess to the gas phase. The formation and growth of these small nanostructures are influenced by the abundance of gas phase molecular precursors such as PAH, hydrocarbon fragments and acetylene which increases with ethylene concentration in the fuel stream. As a consequence of increasing fuel concentration in the ethylene flame series, the flame length increases and thus so does the residence times of nanoparticles in the pyrolytic region. Due to the increased residence time and precursor concentrations, the reaction pathways are likely to lead

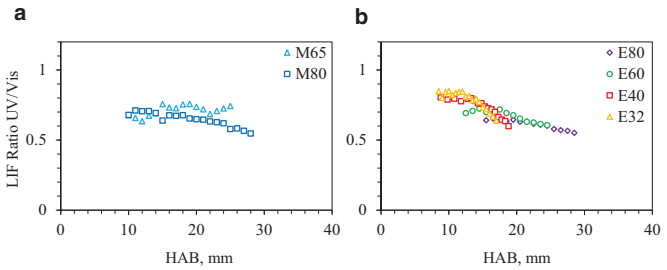

Fig. 6. LIF ratio UV/Visible against HAB (a) methane flames and (b) ethylene flames.

to more abundant and slightly larger nanostructures in the non-incandescent parts of the ethylene flames. It is also worth noting that ELS continues to increase after the first LIE peak and before the onset of significant SVF, suggesting that nanostructures continue to grow in the “dark region” with larger ELS cross-sections, in agreement with previous work [43].

The decay times measured along the centreline of the ethylene flames are presented in Fig. 5(e)–(h), showing that they are larger than those expected for gaseous PAH [23] at the given flame temperatures > 900 K [35]. It is noted here that while there is overall disagreement between the computed and measured temperatures, the location of interest here being the region of initial temperature rise along the centreline shows better agreement [62]. Decay times increase with HAB for all flames, although the E80 flame only shows a marginal increase in and maintains relatively low decay times in comparison to all the other flames studied here. It would be difficult to use decay times to provide details on particle size or structure without further information. ELS, on the other hand, provides an obvious indication that nanostructure size is generally increasing with HAB and in flame conditions that lead to higher SVFs.

Considering only the LIF measurements before the onset of soot by the detection of 1064 nm LII, the evolution of the spectrum emitted by the nanostructures can be explored through the ratio of LIF @ 350 nm and LIF @ 445 nm (UV/VIS). The UV/VIS LIF ratios are presented in Fig. 6 with the two methane flames presented in Fig. 6(a) and ethylene flames in Fig. 6(b). For the non-sooting M65 flame, the UV/VIS ratio remains close to 0.75, after an initial rise, indicating that the LIF spectrum is peaking between 350 nm and 445 nm. The UV/VIS ratio trend suggests that the fluorescent structures on the nanoparticles are primarily comprised of smaller aromatic species not significantly larger than pyrene when comparing this rough spectrum to that of measured PAHs [55,63,64] where, generally speaking, red shifted spectrums correspond to larger aromatics. Furthermore, the resulting spectra are more skewed towards PAHs with a small number of rings when considering the redshift of PAH LIF at high temperatures [23]. Because this ratio does not change with HAB, it indicates that there is no significant evolution in the nanostructures towards more aromatic features when moving downstream. Interestingly this lack of evolution coincides with the absence of detectable 1064 nm LII, suggesting that the evolution toward soot particles from these small nanostructures might need to first step into an aromatisation process, and exhibit a redshift in its spectrum.

In contrast to the M65 flame, the M80 flame ratio is initially close to 0.75 and then decreases moving downstream, indicating a shift in the spectrum towards longer wavelengths and consequently an increase in the size of the dominant aromatic island responsible for LIF, similar to that observed by Hayashida et al. [30]. It could also be possible that these nanostructures evolve towards a more graphitic structure, having layers of small aromatics stacked, as has been found in lower temperature pyrolytic zones [25] which could explain the redshift of the signal. The decrease of

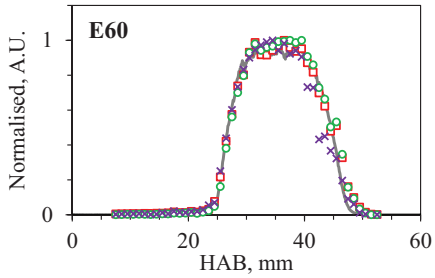

Fig. 7. LII comparison in E60 flame. All measurements are normalised by the maximum value. 1064 nm LII peak (□), 1064 nm LII integrated 0–200 ns (○), 266 nm LIE integrated 60–200 ns (×) and SVF determined from LII (solid line) by Smooke et al. [35]. (For interpretation of the references to colour in this figure legend, the reader is referred to the web version of this article.)

the LIF signal intensity in the downstream region can be attributed partially to a decrease of the quantum yield of the nanostructures, and of course to the evolution towards soot particles, i.e., to larger structures having the capability to emit an LII signal rather than LIF. This second aspect would be confirmed by the rise of the LII just after the decrease of the LIF signal and would follow the known growth pathway for the combustion-generated particles.

All sooting ethylene flames exhibit a similar transition towards a red-shifted spectrum with increasing HAB as shown in Fig 5(b), where the LIF ratio moves to lower values with increasing HAB, a similar trend but a greater shift compared to the sooting M80 flame. In the E60 and E80 flames, the LIF ratio decreases to ultimately lower ratios downstream implying that in the pyrolytic formation of soot, higher soot concentrations are preceded by nanoparticles comprised of aromatic fluorophores with increasing ring numbers and/or more stacked structures. The LIF ratio in the methane and ethylene flames reaches a similarly low value of around 0.55 in both M80 and E80 before the onset of soot, with the E80 flame being much more heavily sooting than M80. The red-shifted spectrum for both the M80 and E80 flames is due in part to the relatively large residence times that these nanostructures have before soot starts and confirms once again the important role of the residence time in the study and the determination of the evolution of the particles in flames.

As seen in Fig. 5, cases E40, E60 and E80 present a dual peak (bimodal structure) in the LIF measurements traced along the length of the flame. Because the 266 nm LIE measurements are being used to quantify the nanostructures based on the LIF signal, it is important to understand if this particular feature is genuine or an artefact due to interferences from other emissions. LII is found to contribute a non-negligible amount to longer integrals (e.g. 0–200 ns) of 266 nm LIE signal even in the flames of lower SVF (E32 and M80).

In order to assess the correlation of the temporal tail of the 266 nm LIE signal with LII excited with 1064 nm and previous SVF measurements [35] a comparison of these signals is shown in Fig. 7. The temporal tail of the 266 nm LIE signal at 575 nm is defined as the integral of the signal between 60 and 200 ns where the LIF contribution of the signal has decayed to negligible values. Both peak and integrated 1064 nm LII signals for the E60 flame are reported which agree well with previous SVF measurements [35]. All curves in Fig. 7 are normalised to have their maximum value of unity. The similarity of all of the curves in Fig. 7 indicates that soot particle size and differences in bath gas composition have a minimal impact on the determination of the relative SVF whether peak, prompt or longer integrated signal are used. Whilst it is common practice to adjust LII and LIE measurements based on temperature to represent volume fraction, it was found that this was unnecessary for the purposes of this investigation. Details of this can be found in the supplementary material and why the authors prefer to leave LIE values unadjusted. The remaining part of the 266 nm LIE signal (0–60 ns) will still contain LII alongside any LIF. In the higher sooting flames (E40, E60, and E80), as seen in Fig. 5, the location of the second LIE peak strongly correlates with the location where 1064 nm LII is measured. Thus, it would be reasonable to assume that a significant portion of this prompt signal in the second peak is driven by the interaction of 266 nm with soot. While LII from 266 nm excitation is expected, the prompt LIF-HAB trend does not completely correlate with 1064 nm LII.

Whilst the second peak in the prompt LIE signal in the highly sooting ethylene flames (see Fig. 5(b)–(d)) cannot be solely attributed to 266 nm LII; it is possible that it is due other interactions of the 266 nm pulse with soot. With the use of 266 nm and particularly at the laser fluence utilised in this work, it would be expected that sublimation and possibly some photo-dissociation processes of soot would lead to the ejection and subsequent excitation of C_2, C_3, carbon clusters and possibly other molecular species resulting in a fast LIE signal. Although care was taken to place the PMTs away from regions in the spectrum known for significant peaks due to C_2 swan bands and C_3 swing bands [53,65], some overlap is possible given the 30 nm collection bin of each PMT. A number of studies using deep UV laser wavelengths (193 nm and 248 nm) have shown that a substantial mass loss and particle disintegration from soot can occur even at modest fluences with little particle heating [45,46,66]. A single photon at 266 nm (37,595 cm^{-1}) does not have enough energy to break a σ bond (43,800 cm^{-1}) between carbon atoms in a soot, whereas a single 193 nm photon does (51,814 cm^{-1}). It is possible that σ bonds could be broken through a multiphoton interaction due to the short 80 ps 266 nm laser pulse.

In order to better understand the signal components from UV excitation where soot is present, the E60 flame at a HAB = 35 mm was explored with a variety of 266 nm laser energies and with a particular focus on the prompt LIE signal in a heavy sooting flame region. The same UV laser and optics as outlined in Section 2 were utilised for this test, so the spot size did not change. However, the laser fluence was varied from 0.11 to 4.2 J/cm^2 by changing the laser energy with a half wave plate thin-film polariser combination.

The response of the LIE signal at 350 nm is presented in Fig. 8(a) in the time domain for a range of fluence levels. The signals are presented with a logarithmic vertical axis to highlight their similar features of the signals over a broad dynamic range. It is evident from Fig. 8(a) that all the signals display a broadly similar behaviour with the initial portion of the signal featuring a fast rise and fall close to the system response limit. The initial fast rise and fall portion of the signal over the first few nanoseconds cannot be attributed to LIF from the same nanostructures observed in other upstream non-sooting regions of the flame as the time decay is much shorter. The initial fast rise and fall portion of the signal is only significant where the SVF is large and thus has not been found as an interference source in previous studies of premixed flames [24] and turbulent flames [40] where SVF levels were much lower. After the initial rapid rise and fall, the signal exhibits a gradual decay that is expected to be from a combination of LIF and LII, with LII dominating the signal at times greater than 20 ns. The LII dominated portion of the signal for all fluence levels displays a similar decay rate, indicating that only a small amount of the total soot mass is sublimated even for the highest fluence case of 4.2 J/cm^2.

In order to quantify the relative emission intensity at different times, the signal for each fluence level is integrated over three different windows in time as presented in Fig. 8(b). The first window from 0 to 3 ns represents the fast rise and fall component, the second window from 3 to 10 ns represents the portion of the signal where nanostructure LIF is expected to be significant. The third window from 60 to 200 ns represents the segment of the sig-

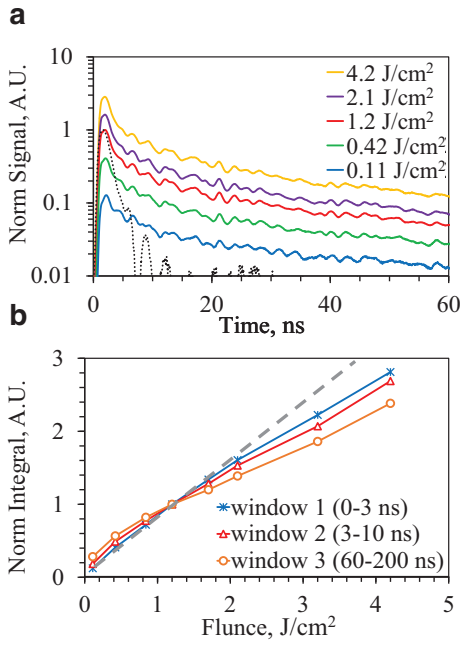

Fig. 8. 266 nm LIE emission @ 350 nm in a high-sooting region for a range of laser fluence levels alongside system response (dotted). (a) Signal level vs. time and (b) relative emission in three temporal windows. (For interpretation of the references to colour in this figure legend, the reader is referred to the web version of this article.)

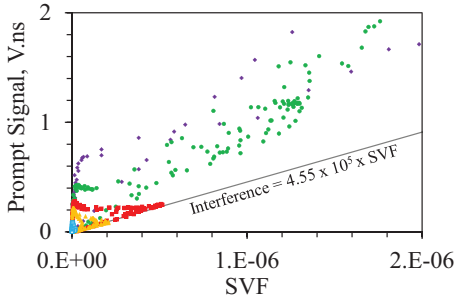

Fig. 9. Scatter plot of prompt LIE vs. SVF. M65 (△), M80 (□), E32 (▲), E40 (■), E60 (●) and E80 (◆). SVF maximum linear interference extrapolated from data (solid line). (For interpretation of the references to colour in this figure legend, the reader is referred to the web version of this article.)

nal that is likely to be exclusively due to LII. The integrated signal in each of the three windows has been normalised such that the integrated signal in each window at a fluence of 1.2 J/cm^2 is unity to be consistent with the fluence used for all other measurements reported in this paper. A dashed line in Fig. 8(b) is shown to indicate what would be an ideal linear response with the laser fluence.

Although the total number of photons received from LII is large over the entire signal duration, the number of photons received from LII in the first window is expected to be relatively low. Such an LII estimate in the first window can be achieved by extrapolating the approximately exponential decay of the LII from later time stages (>20 ns), noting that an exponential decay is a straight line in the log-linear Fig. 8(a). An accurate correction in the time domain for LII interferences is not possible, as there is expected to be a portion of the LII signal that rises and falls rapidly at the system limit response. A fast initial LII signal will be present when the surface of the smallest incandescable soot particles [14,67] is at a temperature sufficiently close to the soot sublimation temperature and the laser pulse is present to drive sublimation. During the laser pulse, it is possible that the smallest particles will be losing significant mass due to sublimation and will produce a strong signal that is only present when the laser pulse is present. The third window in Fig. 8(b) represents the LII, the response of this region with fluence is a power law like with an exponent less than unity, which is expected for an LII process progressing from the linear regime to plateau regime [14,68]. As the spatial profile of the 266 nm beam is Gaussian-like and not strictly a flat-top profile, a region of zero or negative slope with fluence is not observed in Fig. 8(b) even at the highest fluence levels examined.

The signal in the first window displays a near linear trend with the laser fluence up to 1.7 J/cm^2, which indicates that the origin of the signal in this window is not strongly dependent on LII. It is possible the origin of the high-intensity initial portion of the signal is either fluorescence of aromatic compounds coating the soot particles being volatised or excitation of sublimation products. Even for the lowest fluence level examined 0.11 J/cm^2, some sublimation is expected to occur. For fluences larger than 1.7 J/cm^2 in the first window, the sub-linear fluence dependence is due to either saturation effects of the material being fluoresced or the saturation of the mechanism causing the production of the material being fluoresced. Further experiments with additional techniques will be required to definitively determine the origins of the fast high-intensity signal in the first temporal window region.

The signal in the second temporal window features a sub-linear power dependence indicating that there is some LII present in this region but not so much as to completely correlate with the trend observed for the third window that is expected to be exclusively from LII. The signal found in the 3–10 ns region would appear to have a component with a decay time that is comparable to nanostructure LIF found in upstream regions where soot is not present. The prompt signal from 0 to 10 ns which is a combination of the first and second windows in Fig. 8(b) is used for much of the analysis in this paper. As such, it is important to ascertain the nature of any SVF based interferences on this measured whether they are LII based or other mechanisms which is proportional to SVF. An LII signal, even one that decreases quickly due to loss of particle mass, will emit in a quasi-blackbody fashion and thus should emit a larger intensity @ 445 nm than at @ 350 nm, corresponding to a blackbody temperature below or in the range of 3500–4500 K [4,14–18]. Such blackbody emission is not present in Fig. 5(c) and (d), where the prompt LIE @ 350 nm is greater than that @ 445 nm in the sooting regions of E60 and E80 flames. Therefore, based on spectral emission arguments the prompt 266 nm LIE signal that comprises the second peak is without a doubt not solely due to LII.

If the interference on the prompt LIF signal occurs as a result of LII or other mechanisms that are related to the presence of soot, then it is possible a correction can be made for this interference source based on the local SVF. To determine if a relationship between the interference on the prompt LIF and the SVF is consistent for all flames at all locations examined, the prompt LIF signal at 350 nm vs. the SVF is shown in Fig. 9.

The SVF in Fig. 9 is determined from the delayed integral (60 – 200 ns) of the 266 nm LIE measurement at 575 nm as presented in Fig. 7. If all data in Fig. 9 were to sit with minimal scatter on some curve (linear or other) with respect to SVF, then that would indicate that most of the prompt LIF signal is due to interferences from soot. Equally, if a large scatter exists in the data with realisations with very low prompt LIF and large SVF, then that would indicate that there are negligible soot interferences in the prompt LIF signal. However, what is actually found in Fig. 9 is that there is a group of data points sitting on a linear positive slope line which is termed here as the “interference limit line”. Below the interference limit line, no data points are observed and above this line data points with a broad range of

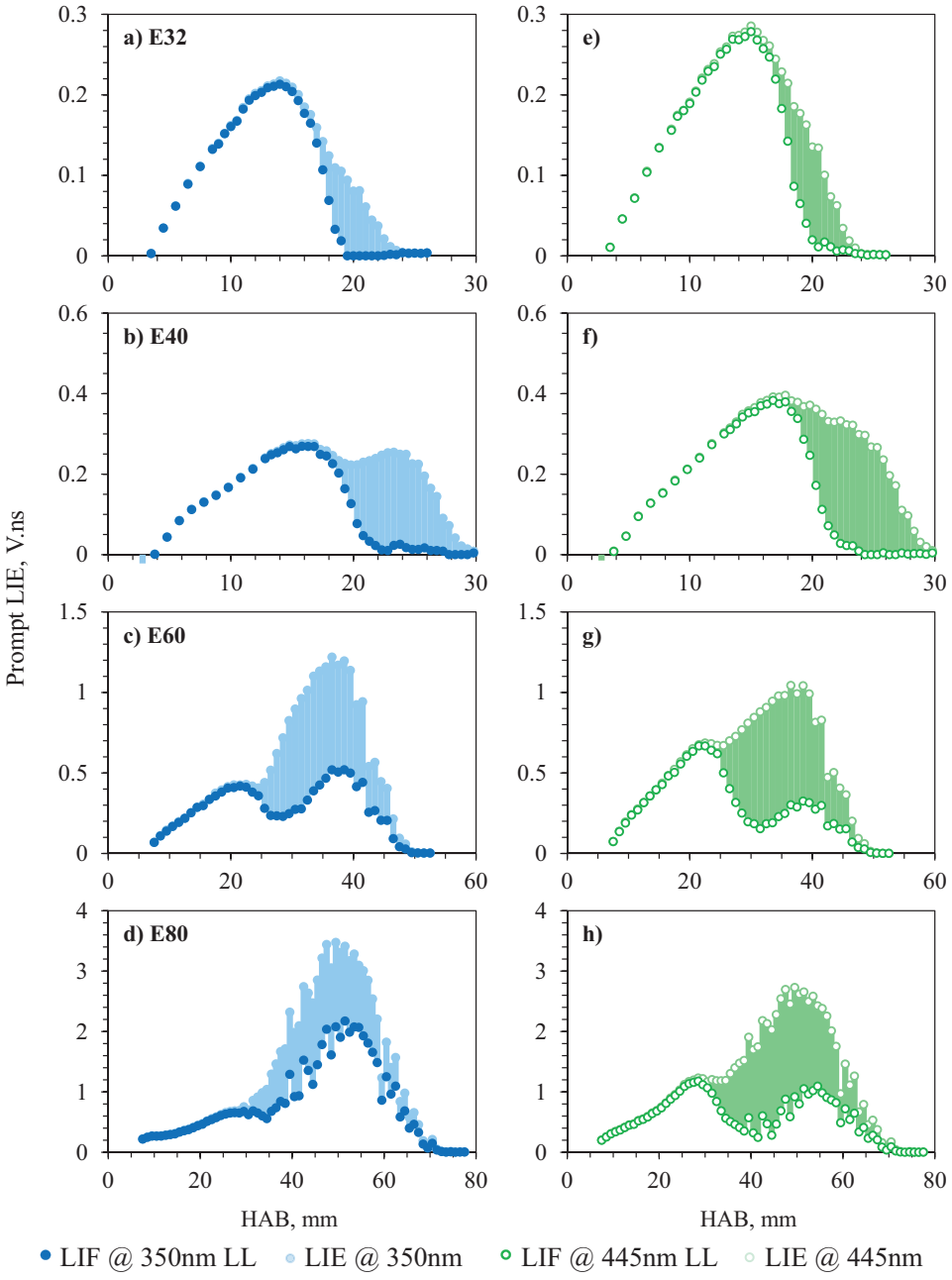

Fig. 10. Lower limit (LL) of prompt LIF centreline measurements corrected for maximum linear interference from SVF for ethylene flames. Uncorrected LIE measurements and shaded area corrected as semi-transparent for comparison.

prompt LIF and SVF values are found. Data along the vertical axis, close to SVF = 0, refers to genuine uncorrupted fluorescence. The interference limit line represents the maximum interference from soot, such that LIE values that lie on the line are potentially 100% soot-derived emissions, whereas values above the line contain some genuine LIF. As the interference limit line is linear, this indicates that the that the prompt LIF interference mechanism is linearly proportional to the SVF, leading to the conclusion that the mechanism for the interference to be more likely due to laser-induced sublimation (a volumetric process) than surface ablation or ejection of volatile compounds from the surface of the soot where a power law relation ($SVF^{2/3}$) would be expected for the interference limit line. As the interference limit line is consistent across all flames at all locations, it indicates that the correction with SVF is essentially independent of the local soot structure for the conditions examined. A similar trend and scatter to the 350 nm data presented in Fig. 9 exists for the prompt LIF @ 445 nm with SVF.

Utilising the interference limit line for the 350 nm and 445 nm PMT data, a correction for soot interferences has been applied to the prompt LIF measurements presented in Fig. 10. The difference before and after the soot interference correction applied to the prompt LIF signal is shown in Fig. 10 to illustrate the region and extent of the correction. It is evident that the SVF correction works well for flames E32 and E40 so that the prompt LIF is reduced to very low levels where soot occurs. Flames E32 and E40 present similar corrected LIF trends to the non-sooting M65 flame and to some extent M80 flame where small amounts of 1064 nm LII is detected. Here there is no second increase of LIF where soot is detected; the LIF signal continues to decrease suggesting an evolution of the small nanostructures into large soot particle and aggregates. A decrease in LIF intensity is also present in the heavier sooting

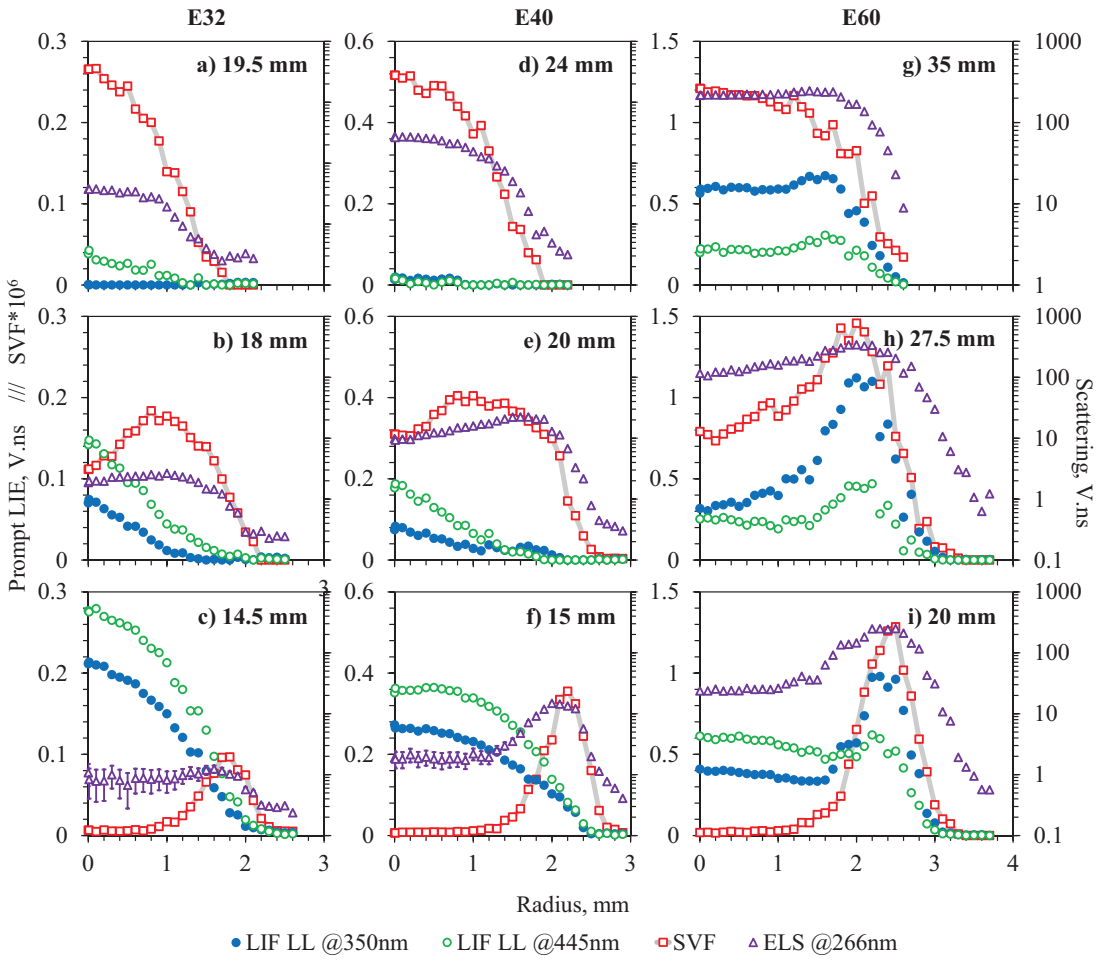

Fig. 11. Prompt LIE and SVF measurements at various HAB against radial position in E32 (a)–(c), E40 (d)–(f) and E60 (g)–(i) and flames. LIF measurements presented have been corrected for maximum linear interference from SVF.

ethylene flames just prior to the second peak and hints at a similar trend of decreasing detectable nanostructure concentration where soot starts to be present in appreciable amounts.

Unlike the trends found in the corrected E32 and E40 flames, the corrected E60 and E80 flames still show a re-increase in LIF downstream in the sooting region, indicating that at least some of the signal contributing to the second peak may be from fluorescent nanostructures. The resurgence of nanostructure LIF in the sooting regions of the E60 and E80 flames does not fit with the picture of particle formation supported by previous studies made in different operating conditions [29,30,69].

A possible explanation for the remaining second LIF peak in the sooting region of the E60 and E80 flames involves the structure of the diffusion flame itself, whereby at downstream locations closer to flame tip, particles from the centreline mix with particles produced in the outer regions or wings of the flame closer to the flame front. To further illustrate this possible transport of material from the wings, Fig. 11 reports the radial profiles for the E32, E40 and E60 at three different HABs, namely at the peak centreline SVF (top), at the maximum soot formation rate i.e. on the maximum increase of the LII signal (middle) and before soot is detected (bottom). The LIF presented in these figures have been corrected for the maximum interference proportional to SVF. These three heights can describe with sufficient precision the spatial evolution of particles within the flame.

For the radial traverses taken at the lowest height for all flames (lower panel in Fig. 11) where no soot is detected on the centreline, it is possible to measure soot on the outer regions, as is evident from the presence of LII wings. Also, for the lowest height cases, the LIF signal in the E32 and E40 flames reaches a maximum on the centreline and decreases with radial distance, whereas in the E60 flame the LIF signal features a local maximum off the centreline in the wing region at the same radial location as the peak SVF. Moving downstream (middle and top panels of Fig. 11), it is seen in the E32 and E40 flames that the radial profiles of LIE decrease in a similar Gaussian-like decay at all axial locations, whereas in the E60 flame the LIF wing peak is still prominent at all axial locations. Similarly, moving to the top panel of the E60 flame, the SVF reaches a maximum on the centreline whereas the 266 nm LIE shows a weak but detectable peak in the flame wing. The position of the LIF peak in the wing region of the E60 flame moves inward with increasing HAB, showing that the reaction zone moves closer to the centreline due to the closure of the flame tip. It can be considered that the material present on or near the tip of the flame is a mixture of material from both the centreline and from the wings of the flame. The presence of strong fluorescence quenching species such as oxygen is to be expected both in the wings as well as near the tip of the flame and would only lead to a reduced fluorescence yield, hence an underestimation of the LIF peak in the wings and tip of the flame.

The longer E60 and E80 flames enables much larger soot concentrations to be formed in the wings due to longer residence times at high temperatures. These features could explain, at least in part, the second peak in the 266 nm LIE signal at the flame tip: the small nanostructures produced on the outer zone are convected toward the flame tip and merge with those coming from

the pyrolytic zone along on the centreline. The observed shift in the importance of particle production and transport from the wings for the high sooting flames agrees with previous results by Smooke et al. [35], which show that the low sooting ethylene flames (E32 and E40) feature a much stronger particle formation on the centreline compared to the higher sooting ethylene E60 and E80 flames where particle production was found to be much higher in the wings. It is worth noting that the formation processes along the centreline compared with that on the wings are likely to be different. The wings of the flame can, in some way, be compared with counter-flow diffusion flames where the mixing of fuel and oxidiser are dominated by diffusion. However, in this coflow diffusion flame, the combustion formed particles in the wings of the flame are convected downstream towards higher HAB experiencing a long residence time in a highly reactive fuel-rich environment. A comparison with similar measurements in a counter-flow flame [25] shows some similarity in the shifting of the spectrum moving towards the oxidiser side. Nanostructures found on the oxidiser side tend to have a blue-shifted spectrum akin to that found in rich premixed conditions [19], where polymerisation of aromatic units into oligomers is favoured. Overall, the measurements and picture formed from the high aspect ratio sooting laminar diffusion flames reported in this paper will help in the understanding of the particle formation pathways and pose a challenge to modellers to successfully predict the origin and evolution of the nanoparticles in these flames. In these nanostructure and transition regions, complementary studies such as electron microscopy, spectrally resolved LIF and TRFPA would likely prove useful in further defining the physical and chemical properties of the nanostructures.

4. Conclusion

In this paper, LIF measurements in combination with LII measurements have proven to be a valuable tool in capturing the transition from aromatic-based nanostructures to soot. From time-resolved measurements, the UV excited LIF signal primarily from condensed phase nanostructures was measured in upstream regions in methane and ethylene coflow diffusion flames.

- The non-sooting M65 flame shows no significant nanostructure evolution before LIF emissions reduce at the oxidative flame tip. However, structural transitions facilitate soot formation even in the marginally sooting M80 flame, where the LIF emission shifts towards a red-shifted spectrum suggesting an increase in the aromatic and stacked nature of the nanostructures.
- A red-shifted spectrum with increasing HAB is also present in the sooting ethylene flames and coincides with a strong increase in ELS. In the upstream regions of these flames, an appreciable scattering signal above the gas phase levels occurs with no measurable SVF, highlighting that the mean nanostructure size must also be increasing with the residence time in the pyrolytic flame region. Close to the soot formation region in these flames, the nanostructures become more graphitic resulting in a reduction in the nanostructure quantum yield hence causing a decrease in the LIF signal level. The nanostructures are known to still be present in this region where LIF intensities decrease and before LII is detected, also known as the “dark region”, as ELS measurements continue to increase with HAB.
- Higher nanostructure concentration is found to proceed the higher SVF found in fuel rich high-sooting flames, although not proportionally, suggesting surface growth strongly contributes to increasing SVF moving downstream.
- LIF measurements become challenging in sooting regions of the flames examined, and interference from LII and other soot derived emissions were found. A linear interference trend with SVF was observed, and corrections for the soot-based interferences were made to the prompt LIF signal. The lower sooting flames (M80, E32 and E40) show LIF signals decreasing to negligible values within the sooting downstream regions well before oxidation at the tip. The longer, heavier sooting flames (E60 and E80) showed a peculiar re-increase in the LIF signal along the centreline in the downstream sooting zone. The presence of LIF from nanostructures in the sooting zone is believed to be genuine and a consequence of the high aspect ratio of these diffusion flames allowing particle formation in the outer regions, or wings, of these flames to be transported downstream to the centreline at the flame tip.
- The particle formation in the outer regions of the flames was identified by a wing structure found in both LIF and LII, where the presence of oxygen and higher temperatures facilitate a different soot formation pathway similar to counter-flow diffusion flames. In the outer regions of the flames less aromatic (blue-shifted spectrum) nanostructures co-exist with larger soot particles and are convected downstream, merging with the centreline. These high aspect ratio diffusion flames pose interesting and challenging features that highlight parallel soot formation pathways.

Acknowledgments

Research at the University of Sydney was supported by supported by the Australian Research Council (project number: DP160105023). Research in Naples was supported by the Accordo di Programma MiSE/CNR “Miglioramento dell’efficienza energetica dei sistemi di conversione locale di energia” 2013–2014 and by Accordo di Programma MiSE/CNR “MiBEST” (PAR 2015 and 2016-17).

Supplementary material

Supplementary material associated with this article can be found, in the online version, at doi:10.1016/j.combustflame.2019.03.026.

References

[1] A. D’Anna, Combustion-formed nanoparticles, Proc. Combust. Inst. 32 (2009) 593–613.
[2] H. Wang, Formation of nascent soot and other condensed-phase materials in flames, Proc. Combust. Inst. 33 (2011) 41–67.
[3] P. Desgroux, X. Mercier, K.A. Thomson, Study of the formation of soot and its precursors in flames using optical diagnostics, Proc. Combust. Inst. 34 (2013) 1713–1738.
[4] H.A. Michelsen, Probing soot formation, chemical and physical evolution, and oxidation: a review of in situ diagnostic techniques and needs, Proc. Combust. Inst. 36 (2017) 717–735.
[5] A. D'Alessio, A. D'Anna, A. D'Orsi, P. Minutolo, R. Barbella, A. Ciajolo, Precursor formation and soot inception in premixed ethylene flames, Symp. (Int.) Combust. 24 (1992) 973–980.
[6] A. D'Alessio, A. D'Anna, G. Gambi, P. Minutolo, The spectroscopic characterisation of UV absorbing nanoparticles in fuel rich soot forming flames, J. Aerosol Sci. 29 (1998) 397–409.
[7] A. Borghese, S.S. Merola, Detection of extremely fine carbonaceous particles in the exhausts of diesel and spark-ignited internal combustion engines, by means of broad-band extinction and scattering spectroscopy in the ultraviolet band 190-400 NM, Symp. (Int.) Combust. 27 (1998) 2101–2109.
[8] L.A. Sgro, G. Basile, A.C. Barone, A. D’Anna, P. Minutolo, A. Borghese, A. D’Alessio, Detection of combustion formed nanoparticles, Chemosphere 51 (2003) 1079–1090.
[9] L.A. Sgro, A.C. Barone, M. Commodo, A. D’Alessio, A. De Filippo, G. Lanzuolo, P. Minutolo, Measurement of nanoparticles of organic carbon in non-sooting flame conditions, Proc. Combust. Inst. 32 (2009) 689–696.
[10] L.A. Sgro, A. De Filippo, G. Lanzuolo, A. D’Alessio, Characterization of nanoparticles of organic carbon (NOC) produced in rich premixed flames by differential mobility analysis, Proc. Combust. Inst. 31 (2007) 631–638.
[11] T.C. Bond, R.W. Bergstrom, Light absorption by carbonaceous particles: an investigative review, Aerosol Sci. Technol. 40 (2006) 27–67.
[12] R.L. Vander Wal, T.M. Ticich, A. Brock Stephens, Can soot primary particle size be determined using laser-induced incandescence? Combust. Flame 116 (1999) 291–296.

[13] G. De Falco, M. Commodo, C. Bonavolonta, G.P. Pepe, P. Minutolo, A. D'Anna, Optical and electrical characterization of carbon nanoparticles produced in laminar premixed flames, Combust. Flame 161 (2014) 3201–3210.
[14] H.A. Michelsen, C. Schulz, G.J. Smallwood, S. Will, Laser-induced incandescence: particulate diagnostics for combustion, atmospheric, and industrial applications, Prog. Energy Combust. Sci. 51 (2015) 2–48.
[15] S. De Iuliis, F. Migliorini, F. Cignoli, G. Zizak, Peak soot temperature in laser-induced incandescence measurements, Appl. Phys. B 83 (2006) 397–402.
[16] F. Goulay, P.E. Schrader, H.A. Michelsen, Effect of the wavelength dependence of the emissivity on inferred soot temperatures measured by spectrally resolved laser-induced incandescence, Appl. Phys. B 100 (2010) 655–663.
[17] D.R. Snelling, K.A. Thomson, F. Liu, G.J. Smallwood, Comparison of LII derived soot temperature measurements with LII model predictions for soot in a laminar diffusion flame, Appl. Phys. B 96 (2009) 657–669.
[18] R. Lemaire, M. Mobtil, Modeling laser-induced incandescence of soot: a new approach based on the use of inverse techniques, Appl. Phys. B 119 (2015) 577–606.
[19] M. Commodo, G. De Falco, A. Bruno, C. Borriello, P. Minutolo, A. D'Anna, Physicochemical evolution of nascent soot particles in a laminar premixed flame: from nucleation to early growth, Combust. Flame 162 (2015) 3854–3863.
[20] H. Bladh, N.E. Olofsson, T. Mouton, J. Simonsson, X. Mercier, A. Faccinetto, P.E. Bengtsson, P. Desgroux, Probing the smallest soot particles in low-sooting premixed flames using laser-induced incandescence, Proc. Combust. Inst. 35 (2015) 1843–1850.
[21] P. Desgroux, A. Faccinetto, X. Mercier, T. Mouton, D. Aubagnac Karkar, A. El Bakali, Comparative study of the soot formation process in a "nucleation" and a "sooting" low pressure premixed methane flame, Combust. Flame 184 (2017) 153–166.
[22] D.B. Kittelson, Engines and nanoparticles: a review, J. Aerosol Sci. 29 (1998) 575–588.
[23] F. Ossler, T. Metz, M. Aldén, Picosecond laser-induced fluorescence from gas-phase polycyclic aromatic hydrocarbons at elevated temperatures. I. Cell measurements, Appl. Phys. B 72 (2001) 465–478.
[24] M. Sirignano, D. Bartos, M. Conturso, M. Dunn, A. D'Anna, A.R. Masri, Detection of nanostructures and soot in laminar premixed flames, Combust. Flame 176 (2017) 299–308.
[25] M. Sirignano, A. Collina, M. Commodo, P. Minutolo, A. D'Anna, Detection of aromatic hydrocarbons and incipient particles in an opposed-flow flame of ethylene by spectral and time-resolved laser induced emission spectroscopy, Combust. Flame 159 (2012) 1663–1669.
[26] B.M. Cetegen, S. Basu, Soot topography in a planar diffusion flame wrapped by a line vortex, Combust. Flame 146 (2006) 687–697.
[27] A. D'Anna, A. Rolando, C. Allouis, P. Minutolo, A. D'Alessio, Nano-organic carbon and soot particle measurements in a laminar ethylene diffusion flame, Proc. Combust. Inst. 30 (2005) 1449–1456.
[28] R.L. Vander Wal, Onset of carbonization: spatial location via simultaneous LIF-LII and characterization via TEM, Combust. Sci. Technol. 118 (1996) 343–360.
[29] R.L. Vander Wal, K.A. Jensen, M.Y. Choi, Simultaneous laser-induced emission of soot and polycyclic aromatic hydrocarbons within a gas-jet diffusion flame, Combust. Flame 109 (1997) 399–414.
[30] K. Hayashida, K. Amagai, K. Satoh, M. Arai, Experimental analysis of soot formation in shooting diffusion flame by using laser-induced emissions, J. Eng. Gas Turbines Power 128 (2006) 241.
[31] A. D'Anna, M. Commodo, M. Sirignano, P. Minutolo, R. Pagliara, Particle formation in opposed-flow diffusion flames of ethylene: an experimental and numerical study, Proc. Combust. Inst. 32 (2009) 793–801.
[32] H.S. Hura, I. Glassman, Fuel oxygen effects on soot formation in counterflow diffusion flames, Combust. Sci. Technol. 53 (1987) 1–21.
[33] S.H. Chung, A. Violi, Insights on the nanoparticle formation process in counterflow diffusion flames, Carbon 45 (2007) 2400–2410.
[34] G. Nathan, International Sooting Flame (ISF) Workshop. http://www.adelaide.edu.au/cet/isfworkshop/ (2017).
[35] M.D. Smooke, M.B. Long, B.C. Connelly, M.B. Colket, R.J. Hall, Soot formation in laminar diffusion flames, Combust. Flame 143 (2005) 613–628.
[36] C.S. McEnally, A.M. Schaffer, M.B. Long, L.D. Pfefferle, M.D. Smooke, M.B. Colket, R.J. Hall, Computational and experimental study of soot formation in a coflow, laminar ethylene diffusion flame, Symp. (Int.) Combust. 27 (1998) 1497–1505.
[37] B.C. Connelly, M.B. Long, M.D. Smooke, R.J. Hall, M.B. Colket, Computational and experimental investigation of the interaction of soot and NO in coflow diffusion flames, Proc. Combust. Inst. 32 (2009) 777–784.
[38] N.J. Kempema, M.B. Long, Quantitative Rayleigh thermometry for high background scattering applications with structured laser illumination planar imaging, Appl. Opt. 53 (2014) 6688–6697.
[39] P.B. Kuhn, B. Ma, B.C. Connelly, M.D. Smooke, M.B. Long, Soot and thin-filament pyrometry using a color digital camera, Proc. Combust. Inst. 33 (2011) 743–750.
[40] D. Bartos, M. Dunn, M. Sirignano, A. D'Anna, A.R. Masri, Tracking the evolution of soot particles and precursors in turbulent flames using laser-induced emission, Proc. Combust. Inst. 36 (2017) 1869–1876.
[41] A. Bruno, C. de Lisio, P. Minutolo, A. D'Alessio, Evidence of fluorescent carbon nanoparticles produced in premixed flames by time-resolved fluorescence polarization anisotropy, Combust. Flame 151 (2007) 472–481.
[42] M. Commodo, F. Ossler, C. de Lisio, A. D'Anna, P. Minutolo, Size measurements of fluorescent carbon nanoparticles in a coflowing laminar diffusion flame by time-resolved fluorescence anisotropy, Combust. Sci. Technol. 184 (2012) 916–928.
[43] M. Commodo, L.A. Sgro, X. Wang, C. De Lisio, P. Minutolo, Fluorescence anisotropy in a diffusion flame to shed light in the 'dark region', Proc. Combust. Inst. 34 (2013) 1845–1852.
[44] H.A. Michelsen, A.V. Tivanski, M.K. Gilles, L.H. Van Poppel, M.A. Dansson, P.R. Buseck, Particle formation from pulsed laser irradiation of soot aggregates studied with a scanning mobility particle sizer, a transmission electron microscope, and a scanning transmission x-ray microscope, Appl. Opt. 46 (2007) 959–977.
[45] C.B. Stipe, J.H. Choi, D. Lucas, C.P. Koshland, R.F. Sawyer, Nanoparticle production by UV irradiation of combustion generated soot particles, J. Nanoparticle Res. 6 (2004) 467–477.
[46] C.B. Stipe, D. Lucas, C.P. Koshland, R.F. Sawyer, Soot particle disintegration and detection by two-laser excimer laser fragmentation fluorescence spectroscopy, Appl. Opt. 44 (2005) 6537–6544.
[47] R.L. Vander Wal, T.M. Ticich, A.B. Stephens, Optical and microscopy investigations of soot structure alterations by laser-induced incandescence, Appl. Phys. B 67 (1998) 115–123.
[48] A. D'Anna, M. Commodo, S. Violi, C. Allouis, J. Kent, Nano organic carbon and soot in turbulent non-premixed ethylene flames, Proc. Combust. Inst. 31 (2007) 621–629.
[49] M. Salamanca, M. Sirignano, A. Danna, Particulate formation in premixed and counter-flow diffusion ethylene/ethanol flames, Energy Fuels 26 (2012) 6144–6152.
[50] M. Salamanca, M. Sirignano, M. Commodo, P. Minutolo, A. D'Anna, The effect of ethanol on the particle size distributions in ethylene premixed flames, Exp. Therm. Fluid Sci. 43 (2012) 71–75.
[51] M. Sirignano, M. Conturso, A. D'Anna, Effect of furans on particle formation in diffusion flames: an experimental and modeling study, Proc. Combust. Inst. 35 (2015) 525–532.
[52] M. Conturso, M. Sirignano, A. D'Anna, Effect of alkylated aromatics on particle formation in diffusion flames: an experimental study, Exp. Therm. Fluid Sci. 73 (2016) 27–32.
[53] P.-E. Bengtsson, M. Aldén, Optical investigation of laser-produced C2 in premixed sooty ethylene flames, Combust. Flame 80 (1990) 322–328.
[54] K.T. Walsh, J. Fielding, M.D. Smooke, M.B. Long, Experimental and computational study of temperature, species, and soot in buoyant and non-buoyant coflow laminar diffusion flames, Proc. Combust. Inst. 28 (2000) 1973–1979.
[55] S. Bejaoui, X. Mercier, P. Desgroux, E. Therssen, Laser induced fluorescence spectroscopy of aromatic species produced in atmospheric sooting flames using UV and visible excitation wavelengths, Combust. Flame 161 (2014) 2479–2491.
[56] K.O. Johansson, T. Dillstrom, P. Elvati, M.F. Campbell, P.E. Schrader, D.M. Popolan-Vaida, N.K. Richards-Henderson, K.R. Wilson, A. Violi, H.A. Michelsen, Radical–radical reactions, pyrene nucleation, and incipient soot formation in combustion, Proc. Combust. Inst. 36 (2017) 799–806.
[57] J.B. Birks, Organic molecular photophysics, J. Wiley, London;New York, 1973.
[58] I.B. Berlman, Handbook of fluorescence spectra of aromatic molecules, Elsevier Science, Burlington, 2012.
[59] Y. Kobayashi, T. Furuhata, K. Amagai, M. Arai, Soot precursor measurements in benzene and hexane diffusion flames, Combust. Flame 154 (2008) 346–355.
[60] R.L. Vander Wal, Soot precursor material: visualization via simultaneous LIF-LII and characterization via tem, Symp. (Int.) Combust. 26 (1996) 2269–2275.
[61] A. D'Anna, M. Sirignano, M. Commodo, R. Pagliara, P. Minutolo, An experimental and modelling study of particulate formation in premixed flames burning methane, Combust. Sci. Technol. 180 (2008) 950–958.
[62] M.D. Smooke, R.J. Hall, M.B. Colket, J. Fielding, M.B. Long, C.S. McEnally, L.D. Pfefferle, Investigation of the transition from lightly sooting towards heavily sooting co-flow ethylene diffusion flames, Combust. Theory Model. 8 (2004) 593–606.
[63] R. Sun, N. Zobel, Y. Neubauer, C. Cardenas Chavez, F. Behrendt, Analysis of gas-phase polycyclic aromatic hydrocarbon mixtures by laser-induced fluorescence, Opt. Lasers Eng. 48 (2010) 1231–1237.
[64] Z. Chi, B.M. Cullum, D.L. Stokes, J. Mobley, G.H. Miller, M.R. Hajaligol, T. Vo-Dinh, Laser-induced fluorescence studies of polycyclic aromatic hydrocarbons (PAH) vapors at high temperatures, Spectrochim. Acta Part A: Mol. Biomol. Spectrosc. 57 (2001) 1377–1384.
[65] F. Goulay, L. Nemes, P.E. Schrader, H.A. Michelsen, Spontaneous emission from C2(d 3Πg) and C3(A 1Πu) during laser irradiation of soot particles, Mol. Phys. 108 (2010) 1013–1025.
[66] J.H. Choi, D. Lucas, C.P. Koshland, Laser ablation of nanoscale particles with 193 nm light, J. Phys.: Conf. Ser. 59 (2007) 54–59.
[67] H.A. Michelsen, Laser-induced incandescence of flame-generated soot on a picosecond time scale, Appl. Phys. B 83 (2006) 443.
[68] H. Bladh, P.E. Bengtsson, J. Delhay, Y. Bouvier, E. Therssen, P. Desgroux, Experimental and theoretical comparison of spatially resolved laser-induced incandescence (LII) signals of soot in backward and right-angle configuration, Appl. Phys. B 83 (2006) 423–433.
[69] C.S. McEnally, L.D. Pfefferle, Experimental study of nonfuel hydrocarbons and soot in coflowing partially premixed ethylene/air flames, Combust. Flame 121 (2000) 575–592.